

# SUV39h-independent association of HP1 $\beta$ with fibrillarin-positive nucleolar regions

Andrea Harničarová Horáková · Eva Bártová ·  
Gabriela Galiová · Radka Uhlířová · Pavel Matula ·  
Stanislav Kozubek

Received: 24 July 2009 / Revised: 4 December 2009 / Accepted: 4 December 2009 / Published online: 23 December 2009  
© Springer-Verlag 2009

**Abstract** Heterochromatin protein 1 (HP1), which binds to sites of histone H3 lysine 9 (H3K9) methylation, is primarily responsible for gene silencing and the formation of heterochromatin. We observed that HP1 $\beta$  is located in both the chromocenters and fibrillarin-positive nucleoli interiors. However, HP1 $\alpha$  and HP1 $\gamma$  occupied fibrillarin-positive compartments to a lesser extent, corresponding to the distinct levels of HP1 subtypes at the promoter of rDNA genes. Deficiency of histone methyltransferases SUV39h and/or inhibition of histone deacetylases (HDACi) decreased HP1 $\beta$  and H3K9 trimethylation at chromocenters, but not in fibrillarin-positive regions that co-localized with RNA polymerase I. Similarly, SUV39h- and HDACi-dependent nucleolar rearrangement and inhibition of rDNA transcription did not affect the association between HP1 $\beta$  and fibrillarin. Moreover, the presence of HP1 $\beta$  in nucleoli is likely connected with transcription of ribosomal genes and with the role of fibrillarin in nucleolar processes.

## Abbreviations

$\mu$ l	Microliter(s)
$\mu$ m	Micrometer(s)
3D	Three-dimensional

BSA	Bovine serum albumin
CD	Chromodomain
CSD	C-terminal chromoshadow domain
DMEM	Dulbecco's modified Eagle's medium
dn	Double null
Dnmt	DNA methyltransferase
FITC	Fluorescein isothiocyanate
GFP	Green fluorescence protein
h	Hour
H3	Histone H3
H1, H2A, H2B, H4	histones H1, H2A, H2B, H4
HDACs	Histone deacetylases
HMTs	Histone methyltransferases
HP1	Heterochromatin protein 1
K (K4, K9, K27...)	Lysine
MEFs	Mouse embryonic fibroblasts
MeCP2	Methyl CpG-binding protein
PBS	Phosphate-buffered saline
PML	Promyelocytic leukemia bodies
RT	Room temperature
RNA Pol I	RNA polymerase I
snoRNAs	Small nucleolar RNAs
wt	Wild type
TSA	Trichostatin A

Communicated by T. Misteli

A. Harničarová Horáková · E. Bártová (✉) · G. Galiová ·  
R. Uhlířová · S. Kozubek  
Institute of Biophysics,  
Academy of Sciences of the Czech Republic,  
v.v.i., Královopolská 135,  
CZ-612 65 Brno, Czech Republic  
e-mail: bartova@ibp.cz

P. Matula  
Faculty of Informatics, Masaryk University,  
Botanická 68a,  
CZ-602 00 Brno, Czech Republic

## Introduction

Nuclear processes such as replication, transcription, splicing, and DNA repair are accompanied by changes in both heterochromatin and euchromatin (Lachner et al. 2003; Lanctôt et al. 2007). The compartmentalization of chromatin is determined by epigenetic events, including DNA

methylation and histone modifications. An important epigenetic mark responsible for the formation of heterochromatin is methylation of histone H3 at lysine 9 (H3K9me), which is mediated by several histone methyltransferases (HMTs), including SUV39h (Lachner et al. 2003; Kouzarides 2007). H3K9 methylation serves as a binding site for heterochromatin protein 1 (HP1), a factor critical for heterochromatin stability (Lachner et al. 2003).

HP1 was first discovered in the pericentromeric and telomeric regions in *Drosophila melanogaster* (James and Elgin 1986; Eissenberg et al. 1990). In the human and mouse genomes, three HP1 subtypes (HP1 $\alpha$ , HP1 $\beta$ , and HP1 $\gamma$ ) have been identified (Saunders et al. 1993). These proteins consist of a highly conserved N-terminal chromodomain (CD) and a C-terminal chromoshadow domain (CSD), which are separated by a hinge region (IVR; Paro and Hogness 1991). The HP1 protein interacts with many partners, including TIF1- $\beta$  (Le Douarin et al. 1996), histone-1-like protein (Nielsen et al. 2001), lamin-B receptor (Ye and Worman 1996), INCENP (Ainsztein et al. 1998), H3K9 methylated sites (Lachner et al. 2003), and others. Dynamic exchange between HP1 protein and chromatin was observed in the living cells, in which HP1 exchange kinetics correlated with the level of chromatin condensation and was influenced by SUV39h deficiency (Cheutin et al. 2003). Moreover, mammalian HP1 subtypes were observed to differ significantly in their nuclear localization, mitotic distribution, and cell cycle-related phosphorylation, according to the cell type (Minc et al. 1999, 2000, 2001; Bártová et al. 2007). For example, various differentiation pathways are characterized by distinct association between HP1 subtypes (Bártová et al. 2007, 2008). HP1 $\alpha$  is mostly found in the centromeres, while HP1 $\beta$  and HP1 $\gamma$  can be found in the centromeres and pericentromeres, as well as the euchromatic sites of the chromosome arms (Minc et al. 1999). In addition, during interphase, all HP1 subtypes were observed to be associated with the promyelocytic leukemia bodies, at varying degrees (Hayakawa et al. 2003). Many of the HP1-interacting partners mentioned earlier were found to bind to the CSD; however, the binding of HP1 to the most prominent histone marker, H3K9 methylation, was observed to be mediated via CD (Lachner et al. 2003; Maison and Almouzni 2004). Thus, the nuclear location of HP1-interacting partners might determine the distribution of HP1 subtypes.

Specific histone variants were observed not only within the particular nuclear regions but also within the nucleoli chromatin. The presence of histone H1 and H2B in the nucleoli have already been described (Allis et al. 1982; Alvarez et al. 2006). Similarly, Erard et al. (1988) showed that histone H1 interacts with the nucleolar protein, nucleolin, in human cells. Using mass spectrometry, the human nucleolus was found to contain several H2A, H2B, and H3

isoforms (Leung et al. 2006; McKeown and Shaw 2009). In the mouse genome, HP1 (subtype was not specified) and H3 methylation (preferentially, H3K9me2), together with other nucleolar complexes, were found to be associated with the methylated rDNA gene promoter (Santoro et al. 2002; Santoro and Grummt 2005). These findings imply that many chromatin-related proteins and nucleolar remodeling complexes, together with histone modifications, regulate the nucleolar processes leading to rRNA synthesis.

## Materials and methods

### Cell cultures

Wild-type Suv39h (wt) and Suv39h double null (dn) mouse embryonic fibroblasts (MEFs) were obtained from the Laboratory of Prof. Thomas Jenuwein (Max-Planck Institute of Immunobiology, Freiburg, Germany). The fibroblasts were cultured in high glucose Dulbecco's modified Eagle's medium (DMEM; #D1152, Sigma-Aldrich, Czech Republic) supplemented with 10% fetal calf serum (PAN, Germany), 100 IU/ml penicillin, and 0.1 mg/ml streptomycin. The pH of the medium was adjusted to 7.2 (500 ml), and 1  $\mu$ l  $\beta$ -mercaptoethanol (Gibco, #31350-010), 5 ml nonessential amino acids (100 $\times$ ; Gibco, #1140-035), 5 ml sodium pyruvate (Gibco, #11360-039), and 1.5 g NaHCO<sub>3</sub> were added to the medium. The cells were treated with Trichostatin A (TSA, 3  $\mu$ M, #T8552, Sigma, Prague, Czech Republic) for 24 or 48 h, and the analyses were performed 24 h after TSA treatment. Suv39h (wt) and SUV39h (dn) cells were treated with 0.5  $\mu$ g/ml Actinomycin D (#A9415, Sigma, Prague, Czech Republic) dissolved in dimethyl sulfoxide (DMSO) for 2 h to suppress transcription. Cells were treated 24 h after plating, along with the addition of fresh medium. Control experiments were performed by adding a relevant amount of DMSO to the cultivation medium. The cells used were cultured under standard conditions at 37°C in a humidified atmosphere containing 5% CO<sub>2</sub>.

Immortalized lamin A/C positive (LMNA wt) and lamin A/C negative (LMNA dn) MEFs were a generous gift from Dr. Teresa Sullivan and Prof. Collin L. Stewart from the Institute of Medical Biology, Singapore. The fibroblasts were cultivated in DMEM supplemented with 10% fetal calf serum at 37°C in humidified atmosphere containing 5% CO<sub>2</sub>. Similar cultivation conditions were used for human small lung carcinoma A549 cells that were purchased from the American Tissue Culture Collection.

### Immunofluorescence

The cells were fixed with 4% formaldehyde for 10 min at room temperature (RT), permeabilized with 0.2% Triton  $\times$ 100

for 10 min and with 0.1% saponin (Sigma, Germany) for 12 min, and were washed twice in phosphate-buffered saline (PBS) for 15 min. We used 1% bovine serum albumin (BSA) dissolved in PBS as the blocking solution. After 1 h of incubation in BSA, the slides were washed for 15 min in PBS, and then incubated with the following antibodies: anti-HP1 $\alpha$  (clone 15.19s, #05-689, Upstate, USA), anti-HP1 $\beta$  (#07-333, Upstate, USA, and #MAB3448, Chemicon International, Germany), anti-HP1 $\gamma$  (clone 42s2, #05-690, Upstate, USA), anti-H3K9me2 (#07-212, Upstate, USA), anti-H3K9me3 (#07-442, Upstate, USA), rabbit polyclonal antibody to fibrillarin (#ab5821, Abcam, UK), and mouse monoclonal antibody to fibrillarin (#ab4566, Abcam, UK). Immunocytochemistry was performed according to Bártošová et al. (2007). After incubation with the primary antibody, the cells were washed twice in PBS for 5 min and incubated for 1 h with the Alexa Fluor SFX Kit (Molecular Probes, Invitrogen detection technologies). In this study, we used the Alexa Fluor 488 Goat Anti-Rabbit SFX kit (#A31627) and the Alexa Fluor 594 Goat anti-mouse SFX Kit (#A31632). The cells were incubated for 1 h at RT. The primary and secondary antibodies were diluted at a ratio of 1:200 (5–10  $\mu\text{g/ml}$ ) in 1% BSA dissolved in PBS. The immunostained cells were washed 3 $\times$  in PBS for 5 min and counterstained with TO-PRO-3 iodide (0.04  $\mu\text{g/ml}$ , Molecular Probes). The location of HP1 $\beta$  inside the nucleoli was verified using two different antibodies, as mentioned earlier (Fig. 2b shows #MAB3448 and Fig. 3b shows #07-333).

Staining with an antibody to RNA polymerase I (RNA Pol I) was done as follows: Cells were grown on cover slips, washed in 1 $\times$  PBS, and then fixed in 4% paraformaldehyde dissolved in 1 $\times$  PBS for 10 min at RT. Cells were then washed twice in 1 $\times$  PBS for 1 min and permeabilized for 15 min at RT in 1% Triton-X-100 dissolved in PBS. The cover slips were then washed twice in PBS for 10 min and blocked in 0.2% gelatine (fish) dissolved in PBS for 15 min. Washing was performed for 15 min in 1 $\times$  PBS. Primary antibody (RPA194, # sc-48385, Santa Cruz, CA, USA) was dissolved at 1:50 in blocking buffer and incubated with the cover slips overnight. The specimens were washed 3 $\times$  in PBS/0.1% Tween for 10 min, and then secondary antibody (Alexa Fluor 594 Goat anti-mouse SFX Kit, #A31632) dissolved in blocking buffer was applied at RT for 1 h. Stained cover slips were kept in a dark chamber and then washed 3 $\times$  in PBS/0.1% Tween for 10 min. TO-PRO-3 iodide was used as a counterstain.

#### Transfection of cells with an expression vector encoding GFP-HP1 $\beta$

The plasmid encoding green fluorescence protein GFP-HP1 $\beta$  was used. Plasmid DNA was isolated by Qiagen Large-Construct kit (#12462, Qiagen, Bio-Consult, Czech

Republic). SUV39h (wt) and SUV39h (dn) cells were transfected using METAFECTENE<sup>TM</sup> PRO system (#T040-0.2; Biontex Laboratories GmbH, Germany) involving purified plasmid DNA. The cells expressing GFP-HP1 $\beta$  were fixed using 4% paraformaldehyde for 10 min, and standard immunofluorescence was performed with mouse monoclonal antibody against fibrillarin (#ab4566, Abcam, UK).

#### Image acquisition

The images were acquired using confocal microscope with Nipkow disc. The system consists of a Leica DMRXA microscope (Leica, Germany) equipped with a confocal head (Yokogawa CSU-10), an argon/krypton laser (Innova 70, Coherent), an acousto-optical tuneable filter (AOTF, Brimrose) for excitation-wavelength selection, Sutter Lambda 10-2 filter exchanger with Chroma filters for emission-wavelength selection, and a CCD camera (Photometrics CoolSNAP HQ CCD camera, UK). Our own in-house software (FISH 2.0) controlled the acquisition system. We acquired several collections of three-dimensional (3D) confocal images, and each collection contained 10 to 20 fields of view of size 1,392 $\times$ 1,040 $\times$ 90 voxels and a resolution of 67 $\times$ 67 $\times$ 100 nm. Every field of view captured a few nuclei (up to five). The image correction and image analysis was carried out using free Acquarium software (see <http://cbia.fi.muni.cz/acquarium>). Fluorescence intensity in the selected genomic regions was also estimated using Andor iQ software (version 1.0.1, ANDOR Technology, South Windsor, CT, USA).

#### Image corrections and image analysis

First, we cut off the individual nuclei from the raw images. Acquarium software automatically placed crop boxes around the nuclei on maximal intensity projection images. We deleted crop boxes that were suggested around low-quality or incomplete nuclei, and subsequently, we cut off the nuclei in a batch. We analyzed the collections of 3D images of individual nuclei using the same experimental strategy (approximately 20 images per collection of typical size of 400 $\times$ 400 $\times$ 90 voxels). We observed an axial chromatic shift between the channels in the order of several slices in our images, and we compensated for the shift using the Acquarium software. We used an automatic shift-correction algorithm on the basis of mutual information registration. The algorithm computes the optimal shift by maximizing the mutual information between the maximal intensity projection images corresponding to different color channels. The axial shift was computed as an arithmetic mean of the suggested shifts for projections along the  $x$ - and  $y$ -axis. If the suggested shifts differed by more than one

slice, i.e., 100 nm, then the user was asked for a manual inspection of the result of the automatic channel alignment.

We analyzed the images of the single nuclei using automatic algorithms. We manually examined the images and checked the segmentation results after the completion of automatic algorithms. If an algorithm made a mistake, then we manually removed the false objects or reanalyzed the problematic images again with different parameters.

#### Nuclei segmentation

Nuclei (blue channel) were segmented using an algorithm based on edge detection (Fig. 1). First, the images were smoothed using a Gaussian filter with anisotropic variance (we used  $\sigma_x=\sigma_y=2$ ,  $\sigma_z=1$  or  $\sigma_x=\sigma_y=4$ ,  $\sigma_z=2$  depending on the quality of images; fast infinite impulse response (IIR) implementation of the Gaussian filtering was used). Subsequently, the magnitude of the image gradient was computed using a central difference approximation formula. The edges were identified as the voxels having a gradient magnitude greater than 2% of the maximal gradient magnitude in the image. The connected components of the edge voxels formed the objects' shells (often with many holes in them). The shells with large bounding boxes (i.e., bounding box volume bigger than 100,000 voxels) were considered to be the nuclear shells. The small shells typically corresponded to chromocenters inside the nucleus. Every big shell was morphologically closed with a spherical structuring element of radius 2  $\mu\text{m}$ . The holes that should have remained in the closed shells were filled on every slice.

#### Chromocenters segmentation

Chromocenters were searched for in the blue (nucleus) channel (Fig. 1). We used multilevel Otsu thresholding

approach for image segmentation. The intensity histogram of the smoothed image (we used IIR Gaussian filter with  $\sigma_x=\sigma_y=1$ ,  $\sigma_z=0.5$ ) within the nucleus mask was analyzed using a two- or three-level Otsu method. Three intensity levels correspond to (1) very dark voxels in the nucleus background representing the nucleoli; (2) bright, densely stained chromocenters; and (3) the remaining chromatin. Always, the most intense class of voxels was assigned as the chromocenters. We applied the Otsu method to the logarithmic histogram (i.e., the logarithm of intensity frequencies was considered in the Otsu algorithm) to some images to increase the success of the threshold determination (especially, if the number of voxels in different intensity clusters was unbalanced). To clarify, bi-level Otsu method assumes that the image contains two classes of voxels: foreground and background. It calculates the optimal threshold separating those two classes so that their intra-class variance is minimal (Otsu 1979). We used a straightforward extension of this method to multilevel grayscale images. The obtained chromocenter components were morphologically opened (Soille 2004) in order to remove small protuberances (smaller than 100 voxels). We used elementary cross (composed of 7 voxels for 3D space) as the structuring element.

#### Nucleoli segmentation

Nucleoli were searched in the red channel within the space identified by the nuclear segmentation (Fig. 1). The intensity histogram of the smoothed image (we used IIR Gaussian filter with  $\sigma_x=\sigma_y=1$ ,  $\sigma_z=0.5$ ) within the nucleus mask was analyzed using the two-level Otsu method. The computed threshold was used for nucleoli segmentation. The obtained nucleoli components were morphologically opened with elementary cross (to remove

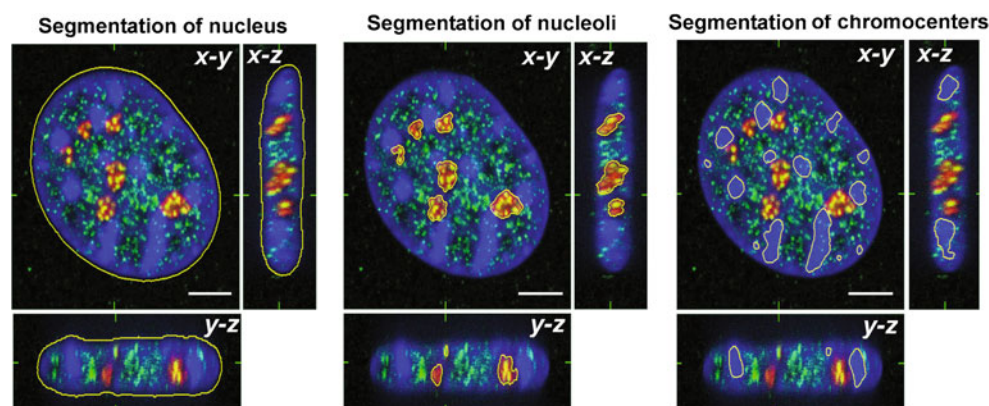


**Fig. 1** An example of automatic segmentation of nuclei, nucleoli, and chromocenters in three-dimensional mode. In this panel,  $x$ - $y$  represents the maximum image, while lateral projections ( $x$ - $z$ ,  $y$ - $z$ ) originate from one confocal view to eliminate overlays that do not

show proper boundaries between the regions studied. Nucleoli were visualized with an antibody against fibrillarin (red); HP1 $\beta$  is shown in green. Nuclei were stained by TO-PRO-3 iodide and pseudo-colored as blue. Scale bars, 1  $\mu\text{m}$

small perturbations), and components smaller than 500 voxels were removed.

#### HP1 content evaluation

We studied the most-frequent intensity value of HP1 channel in the volume of nucleoli and chromocenters. This value indicates the level of HP1 in the studied volume with respect to the other nuclear spaces. We precisely computed the intensity having the highest posterior probability in the volume, and this value was expressed as the percentile of HP1 intensity histogram computed from the whole nucleus. The values close to 100% present evidence of a high concentration of HP1 in the volume. On the other hand, small values indicate a relative deficiency of HP1. Posterior probability distributions were computed using Bayes' formula:  $P(V|I) = P(I|V)P(V)/P(I)$ , where  $P(V|I)$  is the posterior probability that we computed, and  $P(I|V)$  is the probability distribution of intensity  $I$  in the volume  $V$ . It was computed as HP1 intensity histogram at voxels belonging to the considered volume (chromocenters or nucleoli).  $P(I)$  is the probability distribution of intensities within the nucleus and was computed as the intensity histogram of HP1 channel inside the nucleus.  $P(V)$  is the probability that the voxel lies in the studied volume (i.e., being nucleoli voxel or chromocenters voxel) and was computed as the amount of voxels inside the studied volume divided by the number of nucleus voxels. Before the evaluation of the posterior probability according to the Bayes' formula, we smoothed both histograms by a moving average of five.

#### Chromatin immunoprecipitation assays and western blot analysis

ChIP-polymerase chain reaction (PCR) was performed following the protocol published by Strašák et al. (2009). We used appropriate primary antibodies: anti-H3K9 acetylation (#06-942, Upstate, USA), anti-H3K4me2 (#07-030, Upstate, USA), anti-H3K4me3 (#ab8580-2b, Abcam, UK), anti-H3K9me2 (#07-212, Upstate, USA), anti-H3K9me3 (#07-442, Upstate, USA), anti-H3K27me3 (#07-449, Upstate, USA), anti-H3K79me1 (#ab2886-25, Abcam, UK), anti-HP1 $\alpha$  (clone 15.19s, #05-689, Upstate, USA), anti-HP1 $\beta$  (#07-333, Upstate, USA), and anti-HP1 $\gamma$  (clone 42s2, #05-690, Upstate, USA). For ChIP-PCR, we used the primers from Santoro and Grummt (2005), which were specified on the basis of personal communication with Dr. Santoro. The following primers were used: mouse rDNA forward promoter -165/-145: 5'-GACCAGTTGTTCCCTTTGAGG-3', mouse rDNA reverse promoter -20/-1: 5'-ACCTATCTCCAGGTCCAATAG-3' (fragment length was 165 bp) and mouse 28S rDNA forward +8124/8145: 5'-GCGACCTCAGATCAGACGTGG-3', mouse 28S rDNA

reverse +8529/8549: 5'-CTTAACGGTTTCACGCCCTC-3' (fragment length was 426 bp). For amplification, we used Combi PPP Master Mix (Top-Bio, Prague, Czech Republic) and 4% DMSO. We performed 25 cycles of denaturation at 95°C for 30 s, while rDNA promoter primers were annealed at 55°C, and rDNA-encoding 28S rRNA was annealed at 58°C, both for 40 s. The extension temperature was 72°C for 40 s, and finally, we carried out extension at 72°C for 5 min. The PCR reaction was performed using DNA Engine, Peltier Thermal Cycler (Bio-Rad, Hercules, CA, USA). The PCR products were visualized by 2% agarose gel electrophoresis with GelRED (Biotium, #41003, Hayward, CA, USA).

Western blots were performed as in Bártová et al. (2005) and used the following antibodies: anti-H3K9 acetylation (#06-942, Upstate, USA), anti-HP1 $\alpha$  (#05-689, Upstate, USA), anti-HP1 $\beta$  (#07-333, Upstate, USA), anti-HP1 $\gamma$  (#05-690, Upstate, USA), anti-RPA194 (#sc-48385, Santa Cruz, CA, USA), and anti-fibrillarin (#ab5821, Abcam, UK).

#### Quantitative RT-PCR and RNA analysis

Total RNA was isolated using RNAqueous-4PCR kit (Ambion, Applied Biosystems, #AM1914; Invitrogen) according to the manufacturers' protocols. Reverse transcription-PCR was performed following Harničarová Horáková et al. (2009), and we used primers for 28S rDNA, as described above. PCR products were visualized on 1.5% agarose gel running in 1 $\times$  TBE buffer (45 mM Tris-Cl, 45 mM, H<sub>3</sub>BO<sub>3</sub>, 1 mM EDTA, pH8.0). Electrophoresis was performed at 80 V for 3 h.

Analysis of 18S rRNA and 28S rRNA levels was performed on native 1% agarose gel, and for qualification of rRNA levels, we used the following experimental strategy: For each event, total RNA was isolated from 1.5 $\times$ 10<sup>6</sup> cells and then compared on agarose gel.

## Results

### SUV39h deficiency and HDACi reduces the level of HP1 at chromocenters

We utilized immunofluorescence combined with high-resolution Nipkow disc-based confocal microscopy to visualize the localization of some epigenetic factors in control and SUV39h-deficient cells. In addition, the cells were treated with TSA, an inhibitor of histone deacetylases (HDACi). HP1 subtypes were shown to localize at the periphery of the nucleoli, associating with the clusters of pericentromeric heterochromatin called chromocenters (Minc et al. 1999). Thus, we determined how SUV39h deficiency and HDACi influenced the presence of HP1 and H3K9 di- and trimethylation at the chromocenters (Harni-

čarová Horáková et al. 2009). This was then compared to similar epigenetic marks within nucleoli. Analyses of HP1 subtypes confirmed different interphase patterns in SUV39h (wt) and SUV39h (dn) cells (Lehnertz et al. 2003 and Fig. 2a–d). For example, in the control cells, HP1 $\alpha$  was strictly associated with chromocenters (Fig. 2a), while HP1 $\beta$  was observed not only in the chromocenters but also in the chromatin-poor regions in close proximity to the chromocenters (Fig. 2b). HP1 $\gamma$  associated equally with chromocenters and the surrounding chromatin in SUV39h (wt) cells (Fig. 2c). As expected, SUV39h deficiency and HDACi in wt cells significantly reduced the levels of all HP1 subtypes at the chromocenters (Fig. 2a–c, summary Fig. 2d, Harničarová Horáková et al. 2009).

Association of HP1 $\beta$  with fibrillarin-positive regions in the nucleoli is SUV39h- and HDACi-independent

Following elucidation of HP1 nuclear pattern, we examined the presence of all HP1 subtypes inside the nucleoli, which consist of fibrillar centers (FC), dense fibrillar components (DFC), and granular components (summarized by Boisvert et al. 2007). Fibrillarin (ribose 2'-O-methylase), which specifically interacts with small nucleolar RNAs, is located in DFC (Boisvert et al. 2007). In both SUV39h (wt) and SUV39h (dn) cells, the HP1 $\alpha$  and HP1 $\gamma$  subtypes were associated with fibrillarin-positive regions to smaller extent (Fig. 3a, c), when compared with HP1 $\beta$  that strictly colocalized with fibrillarin (Fig. 3b). This nucleolus-

**Fig. 2** Arrangement of HP1 protein subtypes in the interphase nuclei and chromocenters of SUV39h (wt) and SUV39h (dn) cells. The localization of (a) HP1 $\alpha$ , (b) HP1 $\beta$ , and (c) HP1 $\gamma$ . An individual confocal section is shown for each event. Scale bars, 0.5  $\mu$ m. Brightness and contours of individual chromocenters were adjusted with Adobe Photoshop 5.0LE software (blue background was eliminated). **d** Summary of the results; analysis of fluorescence intensity of HP1 subtypes in all the chromocenters of ten nuclei

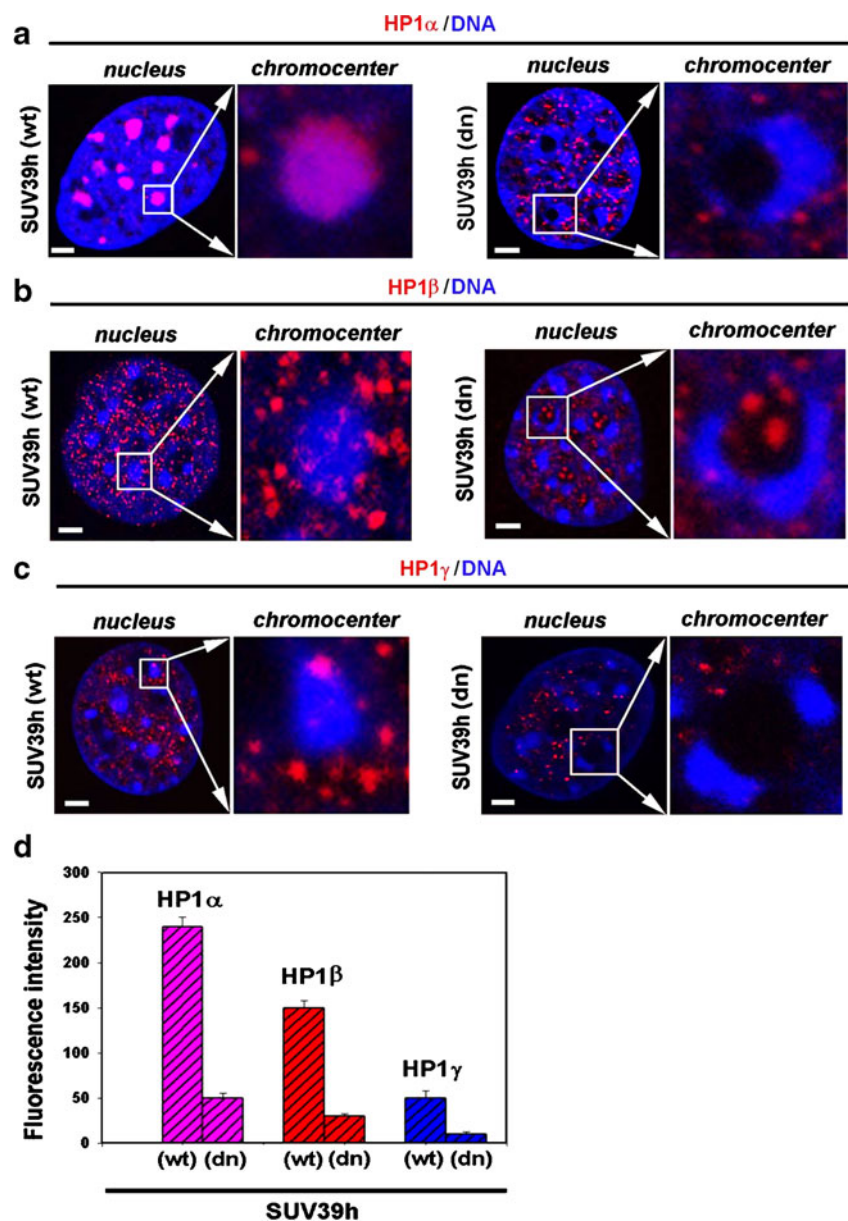
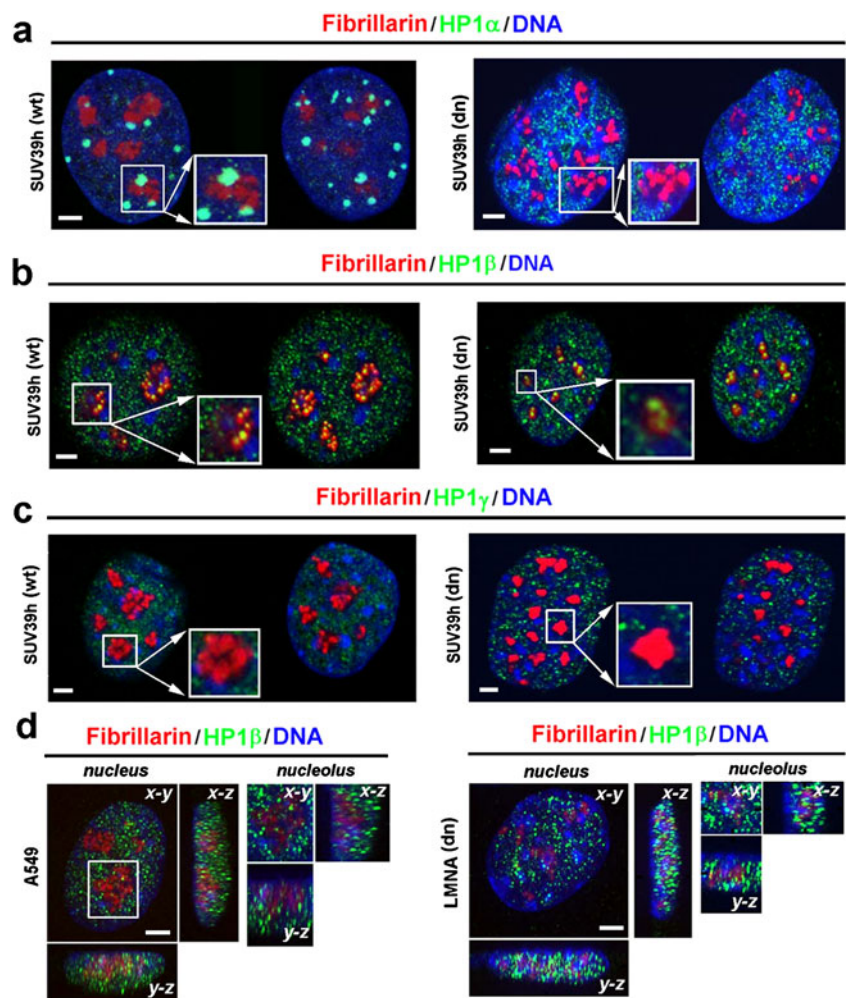


**Fig. 3** Relationship of HP1 subtypes (*green*) to fibrillar-positive regions (*red*) in the nuclei of SUV39h (wt) and SUV39h (dn) cells (*blue*). **a** Nucleoli were visualized with primary antibodies against fibrillarin (*red*); HP1 $\alpha$  is shown in *green*. **b** Presence of HP1 $\beta$  (*green*) and **(c)** low level of HP1 $\gamma$  (*green*) in fibrillar-positive regions (*red*) of the nucleoli in SUV39h (wt) and SUV39h (dn) fibroblasts is shown. Individual confocal sections are provided for each panel. **d** The presence of HP1 $\beta$  (*green*) within the nucleoli (*red*) was observed in A549 cells and LMNA (dn) fibroblasts. Scale bars, 0.5  $\mu$ m



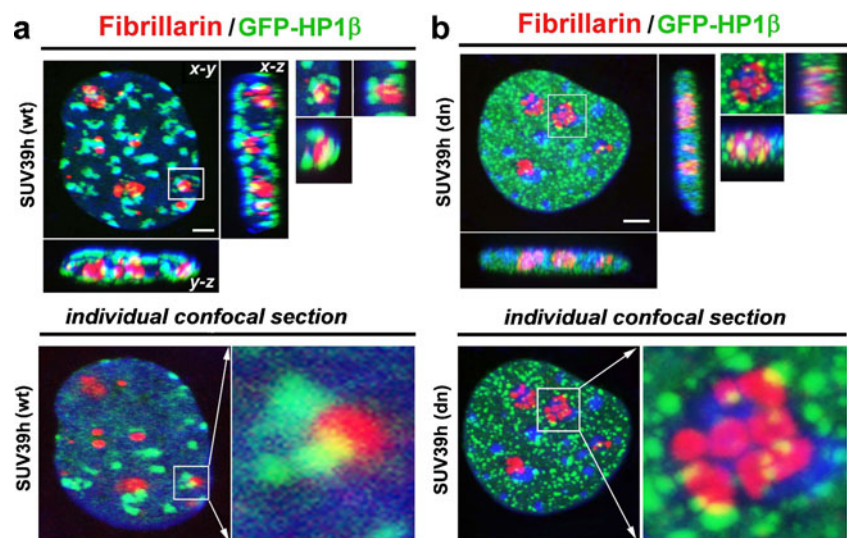
associated location was observed for HP1 $\beta$ , not only in the mouse model studied but also to a lesser extent in human small lung carcinoma A549 cells and mouse fibroblasts lacking the LMNA gene that encodes A-type lamins (Fig. 3d). The association of fibrillar-positive regions with HP1 $\beta$  was also confirmed in SUV39h (wt) and SUV39h (dn) cells transiently expressing GFP-HP1 $\beta$  (Fig. 4). Indeed, we observed a high density of GFP-HP1 $\beta$  protein in fibrillar-positive regions of the nucleoli (Fig. 4a, b). On comparing the nuclear patterns of the endogenous HP1 $\beta$  proteins with those of the same but exogenously expressed nuclear component, we observed particular differences, similar to earlier experiments (Bártová et al. 2007). We found a high level of GFP-HP1 $\beta$  fluorescence at the chromocenters of Suv39h (wt) cells (Fig. 4a), which was different from the diffuse HP1 $\beta$  pattern observed in SUV39h (wt) fibroblasts, as studied by the use of two antibodies against HP1 $\beta$  (Fig. 2b and 3b; “Materials and methods”). The expected absence of this protein at the chromocenters was confirmed in SUV39h (dn) cells transiently expressing GFP-HP1 $\beta$ , while

nucleoli remained densely occupied by GFP-HP1 $\beta$  (Fig. 4b).

In addition to the influence of Suv39h deficiency on the epigenetics and structure of nucleoli, we studied whether HDACi can influence the presence of select epigenetic markers inside the nucleoli (Fig. 5). Both the absence of SUV39h and HDACi decreased H3K9me2 inside the nucleoli, and these changes were more pronounced after TSA treatment of SUV39h (dn) cells (Fig. 5a). On the other hand, we observed that in the fibrillar-positive region, H3K9me3 and HP1 $\beta$  levels were relatively stable compared to the chromocenters of identical cells (Fig. 5b, c). This implies that both Suv39h deficiency and HDAC inhibition have a subtle impact on some epigenetic profiles and epigenetic stability of DFC where fibrillarin is located.

To precisely describe the epigenetics of nucleoli, we performed ChIP-PCR analyses at the rDNA promoter and rDNA sequences encoding 28S rRNA in SUV39h (wt) and SUV39h (dn) fibroblasts (Fig. 6). An abundance of H3K4me2, H3K4me3, H3K9me2, H3K9me3, and H3K27me3 and an absence of H3K79me1 were observed

**Fig. 4** SUV39h (wt) and SUV39h (dn) cells expressing GFP-HP1 $\beta$  and fibrillar localization. **a** SUV39h (wt) and **(b)** SUV39h (dn) fibroblasts transiently expressing GFP-HP1 $\beta$  (green), subsequently stained by antibody against fibrillar (red). In both the cases tested, fibrillar co-localized with HP1 $\beta$  foci. Scale bars represent 1  $\mu$ m



at the selected regions of wt cells (Fig. 6a, b). This observation confirmed that epigenetic markers of active (H3K4me) and inactive (H3K9 and H3K27) chromatin can be found in rDNA genes, which subsequently regulate their transcriptional activity and silencing (Santoro et al. 2002; Santoro and Grummt 2005).

Additional analyses showed that HP1 subtypes occupy rDNA promoter, but not rDNA-encoding 28S rRNA (Fig. 6c). One exception was HP $\gamma$ , which was subtly detected at 28S rDNA in SUV39h (wt) cells. Similarly, TSA caused the presence of HP $\beta$  in this region. In immunostained cells, only HP1 $\beta$  strictly co-localized with

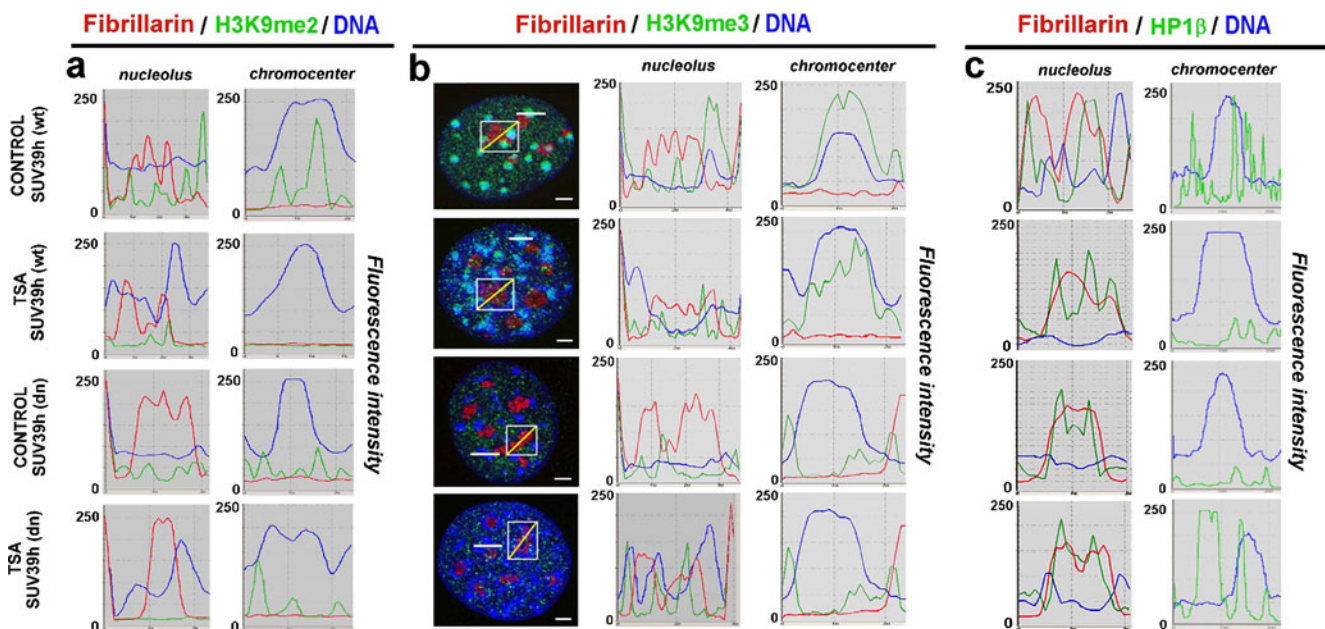


**Fig. 5** Location of H3K9me2, H3K9me3, and HP1 $\beta$  within the nucleoli in control and Trichostatin A (TSA)-treated SUV39h (wt) and SUV39h (dn) fibroblasts. **a** When compared with the control SUV39h (wt) fibroblasts, H3K9me2 levels were decreased inside the nucleoli of SUV39h (dn) cells and in both SUV39h (dn) and SUV39h (wt) cells treated with TSA. Similar results were observed for H3K9me2 at the chromocenters, but H3K9me2 was decreased to a lesser extent at the chromocenters of SUV39h (dn) cells treated by TSA. **b** Fluorescence intensities (in RGB mode) were estimated along the

yellow line in the white frame for nucleoli, and white line for chromocenters. TSA and SUV39h deficiency did not change the presence of H3K9me3 within the nucleoli, while H3K9me3 was reduced at the chromocenters of both control and TSA-treated SUV39h-deficient cells, but not in the chromocenters of TSA-stimulated SUV39h (wt) cells. **c** SUV39h deficiency and hyperacetylation induced by TSA did not change the presence of HP1 $\beta$  within the nucleoli. Scale bars, 0.5  $\mu$ m



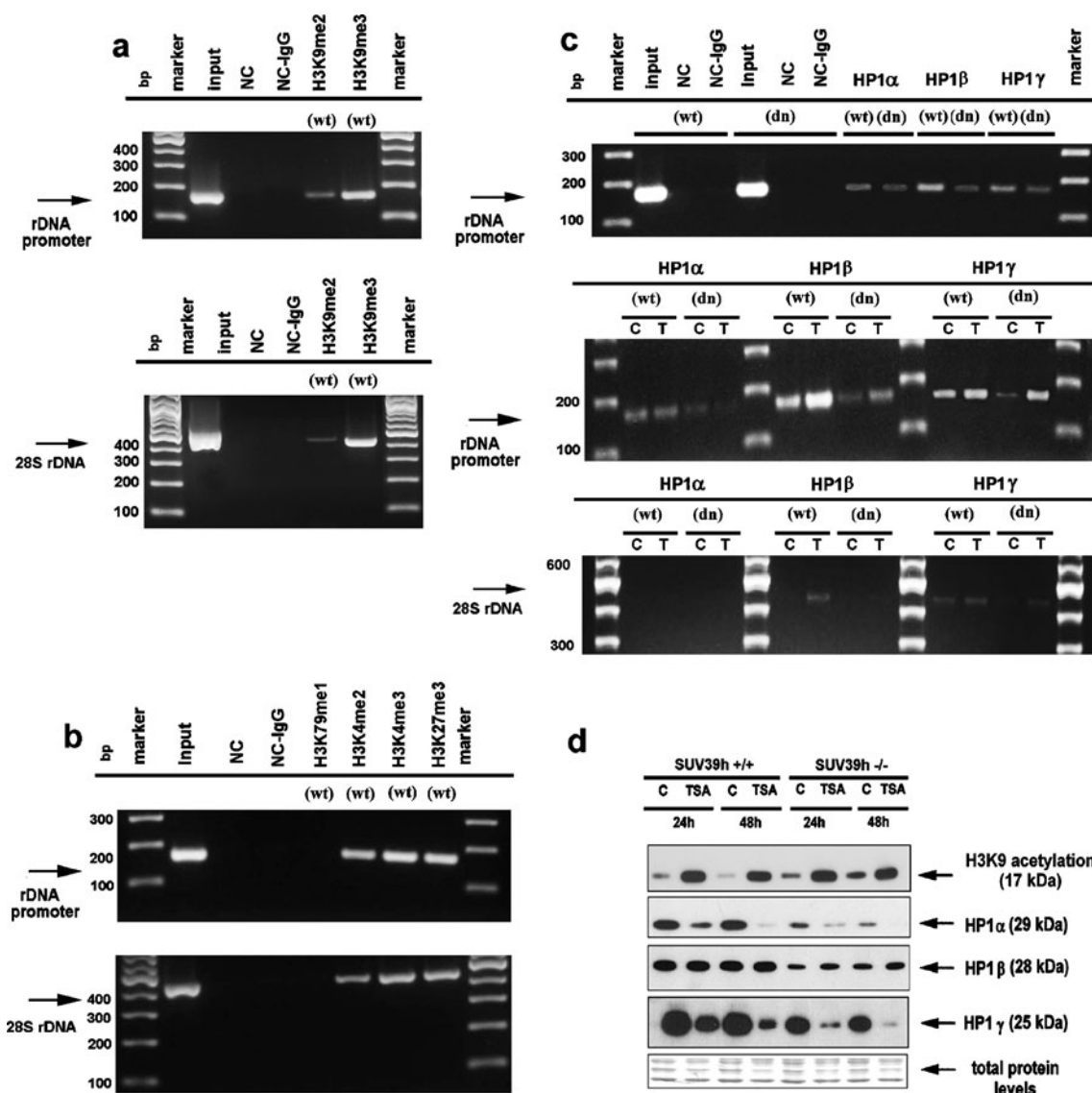


**Fig. 6** ChIP-polymerase chain reaction (PCR) analysis of epigenetic markers in rDNA promoter, rDNA-encoding 28S rRNA, and levels of HP1 subtypes studied by western blot. **a**, **b** H3K4me2, H3K4me3, H3K9me2, H3K9me3, H3K27me3, and H3K79me1 were analyzed in SUV39h (wt) cells by ChIP-PCR. A control reaction was performed in the absence of antibody (NC) and with nonspecific IgG (NC-IgG). **c**

ChIP-PCR analysis of all HP1 subtypes at the promoter of rDNA and rDNA-encoding 28S rRNA in SUV39h (wt) and SUV39h (dn) fibroblasts, including cells treated with Trichostatin A (TSA). Letter C represents control, and T is an abbreviation for TSA-treated cells. **d** Western blot analysis of H3K9 acetylation and HP1 subtypes in the control and TSA-treated SUV39h (wt) and SUV39h (dn) cells

fibrillar-positive DFC, on which boundary transcription of rDNA genes likely proceeds. Conversely, the intensity of HP1 $\alpha$  and HP1 $\gamma$  fluorescence in fibrillar-positive regions was significantly lower compared to the HP1 $\beta$  signals (Fig. 7a). When we compared all HP1 subtypes at the rDNA promoter, the highest level was detected for HP1 $\beta$  in SUV39h (wt) cells, while SUV39h deficiency decreased the level of HP1 $\beta$  at this region (Fig. 6c). Furthermore, our data show that the total amount of HP1 $\beta$  protein is more stable than either HP1 $\alpha$  or HP1 $\gamma$  levels, as determined by western blot. For example, SUV39h (wt) and SUV39h (dn) cells were characterized by significant decreases in global

HP1 $\alpha$  and HP1 $\gamma$ , but not HP1 $\beta$ , after TSA treatment (Fig. 6d; Bártová et al. 2005, 2007). For all HP1 subtypes, we have observed reduced global levels in SUV39h (dn) cells, when compared with (wt) control (Fig. 6d). This correlates with the SUV39h-dependent reduction of HP1 $\beta$  and HP1 $\gamma$  proteins in rDNA promoter (Fig. 6c). Moreover, the decreased levels of HP1 proteins in rDNA promoter corresponds with a reduction in volume and surface of nucleoli in SUV39h (dn) cells (Fig. 7b). Similarly, the level of the large subunit of RNA Pol I (RPA194) was significantly reduced as a result of SUV39h deficiency (1 in Fig. 7c). However, when compared with relevant

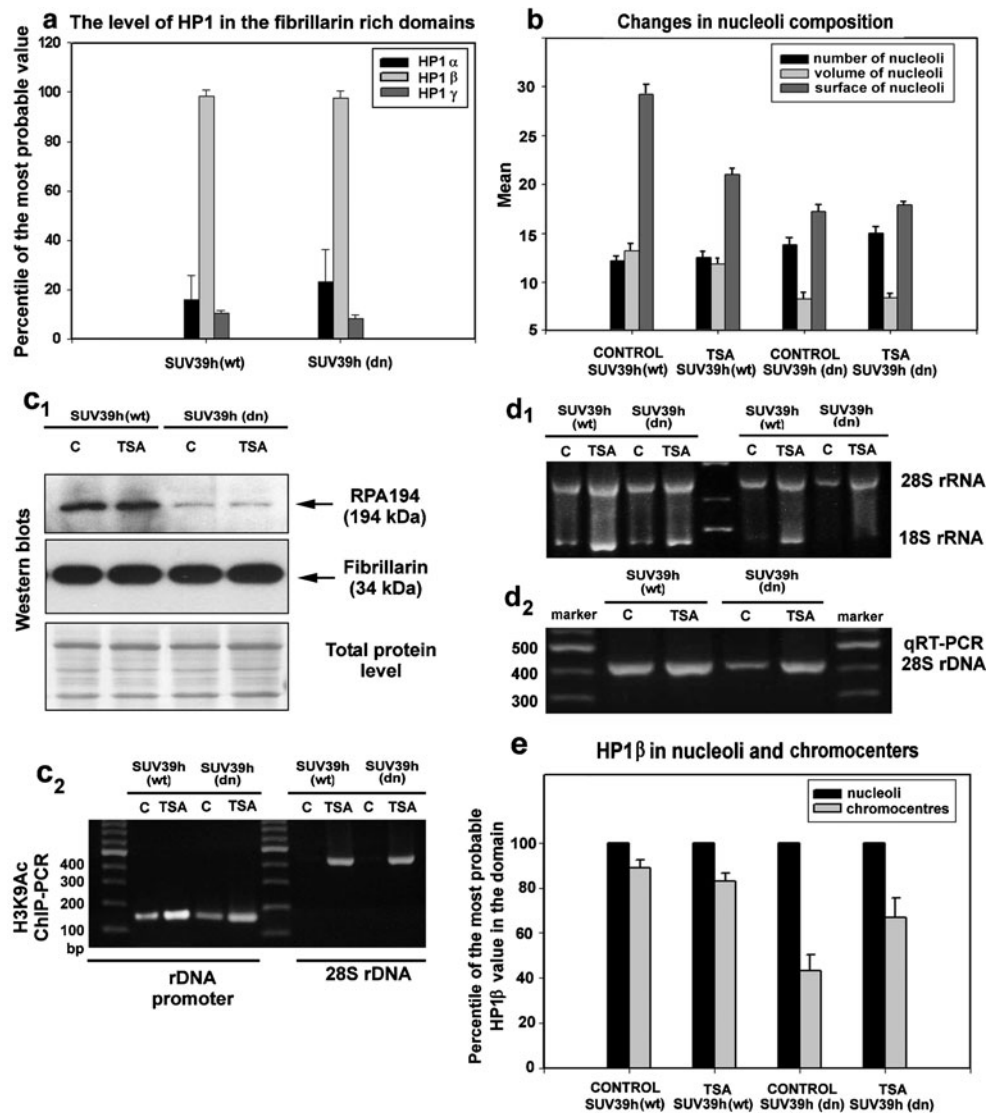


**Fig. 7** Analysis of HP1 protein within the nucleoli undergoing rearrangement. The level of RNA polymerase I (RNA Pol I) was estimated by western blot. **a** Fluorescence intensity of HP1 (HP1 $\alpha$ , HP1 $\gamma$ ) are compared with HP1 $\beta$  in fibrillar-positive domains in SUV39h (wt) and SUV39h (dn) cells. Data are normalized to the interval 0–1 representing the percentile of the average level of HP1 in fibrillar-positive regions in relationship to the average level of HP1 proteins inside the nucleoplasm. **b** Changes in the number, volume, and surface of the nucleoli were estimated using Acquarium software. **c 1** Western blot analysis of the level of the large subunit of RNA Pol I (RPA194, 194 kDa) in control and Trichostatin A (TSA)-treated SUV39h (wt) and

SUV39h (dn) cells. Levels of fibrillarlin (34 kDa) were also estimated by western blot. **c 2** H3K9 acetylation at rDNA promoter and 28S rDNA was studied after TSA treatment. **d 1** Levels of 18S rRNA and 28S rRNA, normalized to  $1.5 \times 10^6$  cells of control and TSA-treated SUV39h (wt) and SUV39h (dn) cell populations. RNA was loaded on the gel twice, 12% of isolated RNA (on the left), then marker, and 8% of isolated RNA (on the right). **d 2** Quantitative reverse transcription-polymerase chain reaction analysis of DNA encoding 28S rRNA. **e** Intensity percentile of the most probable HP1 $\beta$  value in the fibrillar-positive region of nucleoli and in chromocenters of the control and TSA-treated SUV39h (wt) and SUV39h (dn) fibroblasts

controls, the level of RPA194 protein (1 in Fig. 7c) and volume of nucleoli (Fig. 7b) was relatively stable after TSA treatment, while global histone hyperacetylation was induced by TSA (Fig. 6d). This was linked to TSA-dependent increased level of H3K9 acetylation at rDNA promoter and 28S rDNA (2 in Fig. 7c). Taken together, some events, including increased acetylation after TSA and reduced level of RNA Pol I in SUV39h (dn) cells,

corresponds with the TSA-dependent increase and SUV39h-dependent decrease in the level of HP1 $\beta$  and HP1 $\gamma$ , but not HP1 $\alpha$ , at rDNA promoter (Fig. 6c). This data fit together with increased transcription of ribosomal genes after TSA, an in addition, with decreased level of 18S rRNA and 28S rRNA that was observed in SUV39h deficient cells when compared with wt fibroblasts (1 and 2 in Fig. 7d). Taken together, these data provide evidence

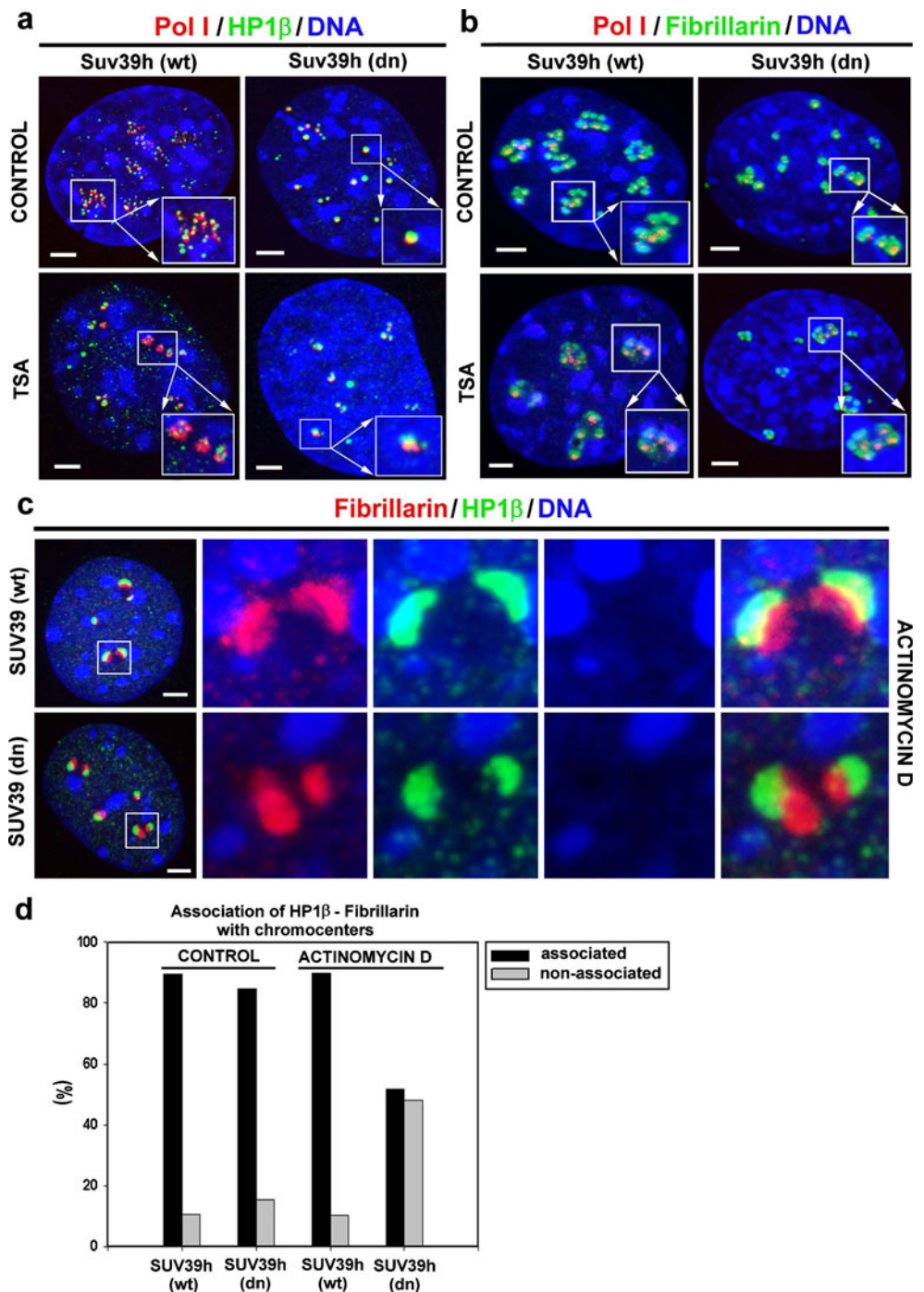
that similar to HP1 $\gamma$  (Yuan et al. 2007), HP1 $\beta$  has likely an important role in rDNA transcription.

Relationship between HP1 $\beta$ -fibrillarin and RNA polymerase I

Immunofluorescence analysis has enabled us to show that the interphase profile of HP1 $\beta$ -fibrillarin complex is not influenced by histone hyperacetylation and SUV39h defi-

ciency, as well (Fig. 7e). This implies that in addition to fibrillarin, HP1 $\beta$  plays important roles in nucleolar processes. When we studied the relationship between RNA Pol I and HP1 $\beta$ , we observed a strict association between the proteins analyzed in control and TSA-treated SUV39h (dn) and SUV39h (wt) cells (Fig. 8a). Similarly, RNA Pol I co-localized with fibrillarin, and this was not influenced by SUV39h deficiency and histone hyperacetylation (Fig. 8b). When transcription of ribosomal genes was blocked by

**Fig. 8** Co-localization of HP1 $\beta$ -fibrillarin and RNA Polymerase I (RNA Pol I). **a** Neither SUV39h deficiency or Trichostatin A-treatment influenced the exact co-localization of (a) HP1 $\beta$  and RNA Pol I nor (b) RNA Pol I and Fibrillarin. **c** Actinomycin D did not change HP1 $\beta$ -fibrillarin association in either SUV39h (wt) or SUV39h (dn) cells. **d** Association of HP1 $\beta$ -fibrillarin complex with chromocenters was reduced in Actinomycin D-treated SUV39h (dn) cells. Bars represent 1  $\mu$ m



Actinomycin D, the association between HP1 $\beta$  and fibrillarin was preserved (Fig. 8c), but it was not as pronounced as observed in non-treated cells (Fig. 3b). Additionally, Actinomycin D caused repositioning of HP1 $\beta$ -fibrillarin complex towards the border of the nucleolar body (Fig. 8c). High stability of fibrillarin was documented by western blot (1 in Fig. 7c). Moreover, HP1 $\beta$  seems to be also the most stable protein of the HP1 subtypes (Fig. 6d). Interestingly, in Actinomycin D-treated SUV39h (wt) cells, we observed that approximately 90% of the HP1 $\beta$ -fibrillarin complexes associated with the nearest chromocenter, similar to control SUV39h (wt) and (dn) fibroblasts, while SUV39h deficiency reduced this association to approximately 50% after Actinomycin D treatment (Fig. 8d).

## Discussion

In this study, we describe the nucleolus, not only as a prominent nuclear structure but also as a region with specific epigenetic features. Indeed, rDNA is characterized by epigenetic markers associated with both transcriptionally active and inactive chromatin, such as acetylation, specific histone methylation, DNA methylation, and the presence of HP1 protein (Santoro et al. 2002; Espada et al. 2007; and the results are shown here). Recent experiments have documented that the histone demethylase, JHDM1B, is located in the nucleolus, where it is responsible for H3K4 demethylation and transcriptional repression (Frescas et al. 2007). Despite the fact that these epigenetic features are similar to that observed within the interphase nuclear chromatin (Lachner et al. 2003), our data clearly show that epigenetic regulation of rDNA genes differs from the epigenetic events that occur within the nucleus, in the non-nucleolar counterparts.

Using automatic segmentation of the nucleoli and chromocenters (see Fig. 1), we provide detailed information about the structural characteristics of selected proteins studied inside the nucleoli and within the chromatin surrounding chromocenters. Our data demonstrate that contrary to the SUV39h-dependent appearance of HP1 proteins within chromocenters, there is an SUV39h- and HDACi-independent structural and functional link between some nucleolar components and the nucleolar epigenome. Occurrence of epigenetic markers, such as H3K9me3 and HP1 $\beta$ , are highly stable in the fibrillarin-positive DFC compared to chromocenters. Moreover, the nucleolar pattern of HP1 $\beta$  could be different from its non-nucleolar counterpart, owing to the fact that the nuclear localization of HP1 protein subtypes has been described as a dynamic process (Cheutin et al. 2003; Festenstein et al. 2003), strongly dependent on SUV39h function (Peters et al.

2002). Furthermore, it was observed that the dynamic properties of HP1, in the non-nucleolar genomic region, play an important role in the maintenance of cell-type specific nuclear architecture that is presumed to dictate many nuclear processes, or vice versa (summarized by Maison and Almouzni 2004).

Owing to co-localization of HP1 $\beta$  with RNA Pol I (Fig. 8a), HP1 $\beta$  appears to be involved in the transcriptional regulation of rDNA genes (compare Figs. 6c and 7c); HP1 $\beta$  and RNA Pol I co-localization is likely independent on SUV39h activity, HDAC inhibition, the number of nucleoli, and level of RNA Pol I subunit RPA194 (Figs. 3b, 5c, and 7b, e). However, decreased levels of HP1 $\beta$  and HP1 $\gamma$  in the promoter of rDNA in SUV39h (dn) cells (Fig. 6c) correlated with decreased levels of an RNA Pol I subunit (1 in Fig. 7c). Similarly, an increase in HP1 $\beta$  and HP1 $\gamma$  in the promoter of rDNA corresponds to increased levels of H3K9 acetylation at rDNA promoter after TSA treatment (compare Fig. 6c with 2 in Fig. 7c). The fact that HP1 $\beta$  co-localized with RNA Pol I (Fig. 8a) implies that HP1 $\beta$  might play an important role in the transcription of ribosomal genes. This is similar to what has been observed for Cockayne syndrome protein B (CSB)-mediated activation of rDNA transcription, which requires the G9a histone methyltransferase responsible for H3K9me1 and H3K9me2 and facilitates the binding of HP1 $\gamma$  (Yuan et al. 2007 and summarized by McStay and Grummt 2008). To clarify, despite the fact that HP1-H3K9 methylation is a well established marker of transcriptionally inactive loci and heterochromatin (Lachner et al. 2003), Yuan et al. (2007) have revealed the presence of HP1 $\gamma$ -H3K9me2, CSB, and RNA Pol I at transcribed regions of acetylated and unmethylated rDNA genes, which is dependent on ongoing transcription. Interestingly, H3K9me3 was observed in both methylated and unmethylated rDNA (Yuan et al. 2007). This is in agreement with our data showing the SUV39h independent appearance of H3K9 trimethylation at fibrillarin-positive regions (Fig. 5b). Moreover, stable HP1 $\beta$  and H3K9 trimethylation profiles within the nucleoli were observed in cells with an A-type lamin deficiency (Fig. 3d) that is responsible for the alteration in HP1 protein and H3K9 methylation in laminopathies (Scaffidi and Misteli 2006; Shumaker et al. 2006).

The role of HP1 $\beta$  in transcription of ribosomal genes was also confirmed by additional results. Our experiments showed that HP1 $\beta$  co-localizes only with the fraction of fibrillarin-positive DFC (Fig. 4), while more pronounced co-localization was observed for HP1 $\beta$  and the RNA Pol I subunit (RPA194; Fig. 8a). However, certain proportion of HP1 $\beta$  appeared outside RPA194-positive regions. These results likely imply that HP1 $\beta$  is involved primarily in the RNA Pol I regions with some extensions to the periphery of fibrillarin-positive DFCs. This protein relationship was

even more pronounced in nucleoli under Actinomycin D treatment, which partially separates the RNA Pol I regions from fibrillarin and Nopp140-positive DFCs (Chen et al. 1999). Interestingly, the Actinomycin D-dependent pattern of co-localization between HP $\beta$  and fibrillarin (Fig. 8c) significantly corresponds to the pattern of RNA Pol I and Nop140, as observed by Chen et al. (1999). Based on these results, we suggest that co-localization of HP1 $\beta$  with fibrillarin is limited (Fig. 8c), which was confirmed by following experiments: In wt cells, HP1 $\beta$  strictly co-localized with fibrillarin (Fig. 3b), while Actinomycin D caused only partial association of these proteins (Fig. 8c). These observations could possibly explain HP1 $\beta$  detection at the ribosomal DNA promoters since the periphery of the FC and DFC is considered as a site of active ribosomal DNA transcription (Dundr and Raška 1993; Hozák et al. 1999).

Recent studies highlighted the dynamic nature of the nucleoli, whose composition can vary under different nuclear pathophysiological conditions leading to multiple genetic disorders and cancer (Boisvert et al. 2007). In this study, we also observed significant rearrangement of the nucleoli (Fig. 7b), but surprisingly, the nucleolar epigenome was relatively stable and less sensitive to the intranuclear stimuli than the surrounding chromatin. This may also explain the importance of the nucleolar factors in the physiological embryonic development that requires proper nucleolar function (Ogushi et al. 2008). The nucleolus is eliminated during spermiogenesis, and thus, the nucleolus is exclusively maternally inherited via the oocyte. Moreover, Ogushi et al. (2008) showed that the maternal nucleolus from the somatic cell nuclear transfer is essential for successful embryonic development. Considering these data, we suggest that not only the chromatin-remodeling factors involved in the nucleolus but also the highly stable and specific epigenome of the nucleoli may control rRNA synthesis, and thus, embryogenesis.

On the other hand, epigenetic profiles of the chromocenters were significantly influenced by SUV39h deficiency (Lehnertz et al. 2003; Harničarová Horáková et al. 2009; Fig. 2). We confirmed the results of Lehnertz et al. (2003) and Taddei et al. (2001) that show that SUV39h deficiency and hyperacetylation are associated with a reduction of all HP1 subtypes at the chromocenters and/or disassembly of the HP1 protein with these nuclear regions, as induced by TSA (Taddei et al. 2001; Bártová et al. 2005). A similar dissociation was observed between HP1 $\beta$ –fibrillarin complex and chromocenters in SUV39h (dn) cells treated with Actinomycin D (Fig. 8d). Conversely, chromocenter-associated H3K9me3 was found to be stable following TSA-induced hyperacetylation in SUV39h (wt) cells (Fig. 5b). Thus, we assume that the HP1 protein subtypes are a more flexible fraction of the nucleus than H3K9 trimethylation. Our data also support the conclusion that

H3K9me3 is not the exclusive HP1-binding partner. Other factors, for example, DNA methyltransferases (Dnmts), G9a HMT, TIF1 $\beta$ , and/or methyl CpG-binding protein, are considered to be additional HP1-interacting proteins (Singh and Georgatos 2002; Cammas et al. 2002; Bártová et al. 2007). This coincides with the statement of Espada et al. (2007) about the Dnmt1-dependent mechanism for the structural organization of the nucleolar compartment. Moreover, Dnmt1 was shown to be a prominent HP1-interacting partner (Smallwood et al. 2007); thus, Dnmt1 is also presumed to be responsible for the relatively stable epigenomes of nucleoli. On the other hand, H3K9me2 inside nucleoli was significantly reduced in our experimental system (Fig. 5a). This correlated well with an observation made by Peng and Karpen (2007) that mutation in *Su (var)3-9* (a homolog of mouse Suv39h) in *D. melanogaster* results in decreased levels of H3K9me2, disorganization of the nucleoli, rDNA, and satellite DNAs.

Taken together, our results imply that HP1 $\beta$  and H3K9me3, but not H3K9me2, localize to the fibrillarin-positive DFC in a SUV39h- and histone acetylation-independent manner. This was different from the HP1 $\beta$ –H3K9me3 and H3K9me2 pattern in chromocenters, the epigenetic pattern of which is influenced by SUV39h deficiency and hyperacetylation. On the other hand, we realize that Suv39h HMTs are not the only enzymes responsible for H3K9 methylation and HP1 binding (summarized by Kouzarides 2007). Here, we show that HP1 $\beta$  is likely involved in transcription of ribosomal genes that is decreased in SUV39h deficient cells (1 and 2 in Fig. 7d) in parallel with a reduced level of HP1 $\beta$  at rDNA promoter. Moreover, fibrillarin, which acts as a ribose 2'-O-methylase in RNA modification, is presumed to regulate some epigenetic processes within the nucleolus, as it co-localizes with HP1 $\beta$ . We suggest that physiological role of HP1 $\beta$  is likely linked with transcription of ribosomal genes and with fibrillarin-associated functions, such as pre-rRNA processing, rRNA modification, and ribosome biosynthesis (Jansen et al. 1991; Boisvert et al. 2007).

**Acknowledgments** This work was supported by the research projects: LC535, LC06027, ME919, AVOZ50040702, AVOZ50040507, 2B06052, and 1QS500040508. We thank Prof. Thomas Jenuwein and Dr. Suzane Opravil for providing us the SUV39h-deficient cells, and Dr. Teresa Sullivan and Prof. Collin L. Stewart for LMNA (dn) fibroblasts. We also thank Dr. R. Santoro for providing the rDNA and 28S rDNA primer sequences and Dr. Monika Lachner for the valuable comments of our manuscript. GFP-HP1 $\beta$  plasmid was a generous gift from Dr. Tom Misteli, Laboratory of Receptor Biology and Gene Expression, National Institute of Health, Bethesda. We are also grateful to Dr. Laney Weber from BioScience Writers (Houston, TX, USA) and SPi editing service for the critical revision of our manuscript. Many thanks to Dr. Joost Zomerdijk (from Wellcome Trust Centre for Gene Regulation and Expression, College of Life Sciences, University of Dundee, UK) for recommending the antibody against the large RNA Pol I subunit (RPA194).

**Conflict of interest statement** The authors declare that they have no conflict of interest.

## References

- Ainsztein AM, Kandels-Lewis SE, Mackay AM, Earnshaw WC (1998) INCENP centromere and spindle targeting: identification of essential conserved motifs and involvement of heterochromatin protein HP1. *J Cell Biol* 143:1763–1774
- Allis CD, Ziegler YS, Gorovsky MA, Olmsted JB (1982) A conserved histone variant enriched in nucleoli of mammalian cells. *Cell* 31:131–136
- Alvarez M, Quezada C, Molina A, Krauskopf M, Vera MI, Thiry M (2006) Ultrastructural changes of the carp (*Cyprinus carpio*) hepatocyte nucleolus during seasonal acclimatization. *Biol Cell* 98:457–463
- Bártová E, Pacherník J, Hamičarová A, Kovařík A, Kovaříková M, Hofmanová J, Skalníková M, Kozubek M, Kozubek S (2005) Nuclear levels and patterns of histone H3 modification and HP1 proteins after inhibition of histone deacetylases. *J Cell Sci* 118:5035–5046
- Bártová E, Pacherník J, Kozubík A, Kozubek S (2007) Differentiation-specific association of HP1alpha and HP1beta with chromocentres is correlated with clustering of TIF1β at these sites. *Histochem Cell Biol* 127:375–388
- Bártová E, Galiová G, Krejčí J, Hamičarová A, Strašák L, Kozubek S (2008) Epigenome and chromatin structure in human embryonic stem cells undergoing differentiation. *Differentiation* 76:24–32
- Boisvert FM, van Koningsbruggen S, Navascués J, Lamond AI (2007) The multifunctional nucleolus. *Nat Rev Mol Cell Biol* 8:574–858
- Cammas F, Oulad-Abdelghani M, Vonesch JL, Huss-Garcia Y, Chambon P, Losson R (2002) Cell differentiation induces TIF1β association with centromeric heterochromatin via an HP1 interaction. *J Cell Sci* 115:3439–3448
- Chen HK, Pai CY, Huang JY, Yeh NH (1999) Human Nopp 140, which interacts with RNA polymerase I: implications for rRNA gene transcription and nucleolar structural organization. *Mol Cell Biol* 19:8536–8546
- Cheutin T, McNairn AJ, Jenuwein T, Gilbert DM, Singh PB, Misteli T (2003) Maintenance of stable heterochromatin domains by dynamic HP1 binding. *Science* 299:721–725
- Dundr M, Raška I (1993) Nonisotopic ultrastructural mapping of transcription sites within the nucleolus. *Exp Cell Res* 208:275–281
- Eissenberg JC, James TC, Foster-Hartnett DM, Hartnett T, Ngan V, Elgin SC (1990) Mutation in a heterochromatin-specific chromosomal protein is associated with suppression of position-effect variegation in *Drosophila melanogaster*. *Proc Natl Acad Sci USA* 87:9923–9927
- Erard MS, Belenguer P, Caizergues-Ferrer M, Pantaloni A, Amalric F (1988) A major nucleolar protein, nucleolin, induces chromatin decondensation by binding to histone H1. *Eur J Biochem* 175:525–530
- Espada J, Ballestar E, Santoro R, Fraga MF, Villar-Garea A, Németh A, Lopez-Serra L, Roper S, Aranda A, Orozco H, Moreno V, Juarranz A, Stockert JC, Längst G, Grummt I, Bickmore W, Esteller M (2007) Epigenetic disruption of ribosomal RNA genes and nucleolar architecture in DNA methyltransferase 1 (Dnmt1) deficient cells. *Nucleic Acids Res* 35:2191–2198
- Festenstein R, Pagakis SN, Hiragami K, Lyon D, Verreault A, Sekkali B, Kioussis D (2003) Modulation of heterochromatin protein 1 dynamics in primary mammalian cells. *Science* 299:719–721
- Frescas D, Guardavaccaro D, Bassermann F, Koyama-Nasu R, Pagano M (2007) JHDM1B/FBXL10 is a nucleolar protein that represses transcription of ribosomal RNA genes. *Nature* 450:309–313
- Harničarová Horáková A, Galiová G, Legartová S, Kozubek S, Matula P, Bártová E (2009) Chromocentre integrity and epigenetic marks. *J Struct Biol* (in press)
- Hayakawa T, Haraguchi T, Masumoto H, Hiraoka Y (2003) Cell cycle behavior of human HP1 subtypes: distinct molecular domains of HP1 are required for their centromeric localization during interphase and metaphase. *J Cell Sci* 116:3327–3338
- Hozák P, Cook PR, Schöfer C, Mosgöller W, Wachtler F (1994) Site of transcription of ribosomal RNA and intranucleolar structure in HeLa cells. *J Cell Sci* 107(Pt 2):639–648
- James TC, Elgin SC (1986) Identification of a nonhistone chromosomal protein associated with heterochromatin in *Drosophila melanogaster* and its gene. *Mol Cell Biol* 6:3862–3872
- Jansen RP, Hurt EC, Kern H, Lehtonen H, Carmo-Fonseca M, Lapeyre B, Tollervey D (1991) Evolutionary conservation of the human nucleolar protein fibrillarin and its functional expression in yeast. *J Cell Biol* 113:715–729
- Kouzarides T (2007) Chromatin modifications and their function. *Cell* 128:693–705
- Lachner M, O'Sullivan RJ, Jenuwein T (2003) An epigenetic road map for histone lysine methylation. *J Cell Sci* 116:2117–2124
- Lancôt C, Cheutin T, Cremer M, Cavalli G, Cremer T (2007) Dynamic genome architecture in the nuclear space: regulation of gene expression in three dimensions. *Nat Rev Genet* 8:104–115
- Le Douarin B, Nielsen AL, Garnier JM, Ichinose H, Jeanmougin F, Losson R, Chambon P (1996) A possible involvement of TIF1 alpha and TIF1 beta in the epigenetic control of transcription by nuclear receptors. *EMBO J* 15:6701–6715
- Lehnertz B, Ueda Y, Derijck AA, Braunschweig U, Perez-Burgos L, Kubicek S, Chen T, Li E, Jenuwein T, Peters AH (2003) Suv39h-mediated histone H3 lysine 9 methylation directs DNA methylation to major satellite repeats at pericentric heterochromatin. *Curr Biol* 13:1192–1200
- Leung AK, Trinkle-Mulcahy L, Lam YW, Andersen JS, Mann M, Lamond AI (2006) NOPdb: nucleolar proteome database. *Nucleic Acids Res* 34:D218–D220 (Database issue)
- Maison C, Almouzni G (2004) HP1 and the dynamics of heterochromatin maintenance. *Nat Rev Mol Cell Biol* 5:296–304
- McKeown PC, Shaw PJ (2009) Chromatin: linking structure and function in the nucleolus. *Chromosoma* 118:11–23
- McStay B, Grummt I (2008) The epigenetics of rRNA genes: from molecular to chromosome biology. *Annu Rev Cell Dev Biol* 24:131–157
- Minc E, Allory Y, Worman HJ, Courvalin JC, Buendia B (1999) Localization and phosphorylation of HP1 proteins during the cell cycle in mammalian cells. *Chromosoma* 108:220–234
- Minc E, Courvalin JC, Buendia B (2000) HP1gamma associates with euchromatin and heterochromatin in mammalian nuclei and chromosomes. *Cytogenet Cell Genet* 90:279–284
- Minc E, Allory Y, Courvalin JC, Buendia B (2001) Immunolocalization of HP1 proteins in metaphasic mammalian chromosomes. *Methods Cell Sci* 23:171–174
- Nielsen AL, Oulad-Abdelghani M, Ortiz JA, Remboutsika E, Chambon P, Losson R (2001) Heterochromatin formation in mammalian cells: interaction between histones and HP1 proteins. *Mol Cell* 7:729–739
- Ogushi S, Palmieri C, Fulka H, Saitou M, Miyano T, Fulka J Jr (2008) The maternal nucleolus is essential for early embryonic development in mammals. *Science* 319:613–616
- Otsu N (1979) A threshold selection method from gray-level histograms. *IEEE Trans Syst Man Cybern* 9:62–66
- Paro R, Hogness DS (1991) The Polycomb protein shares a homologous domain with a heterochromatin-associated protein of *Drosophila*. *Proc Natl Acad Sci USA* 88:263–267

- Peng JC, Karpen GH (2007) H3K9 methylation and RNA interference regulate nucleolar organization and repeated DNA stability. *Nat Cell Biol* 9:19–20
- Peters AH, Mermoud JE, O'Carroll D, Pagani M, Schweizer D, Brockdorff N, Jenuwein T (2002) Histone H3 lysine 9 methylation is an epigenetic imprint of facultative heterochromatin. *Nat Genet* 30:77–80
- Santoro R, Grummt I (2005) Epigenetic mechanism of rRNA gene silencing: temporal order of NoRC-mediated histone modification, chromatin remodeling, and DNA methylation. *Mol Cell Biol* 25:2539–2546
- Santoro R, Li J, Grummt I (2002) The nucleolar remodeling complex NoRC mediates heterochromatin formation and silencing of ribosomal gene transcription. *Nat Genet* 32:393–396
- Saunders WS, Chue C, Goebel M, Craig C, Clark RF, Powers JA, Eissenberg JC, Elgin SC, Rothfield NF, Earnshaw WC (1993) Molecular cloning of a human homologue of *Drosophila* heterochromatin protein HP1 using anti-centromere autoantibodies with anti-chromo specificity. *J Cell Sci* 104:573–582
- Scaffidi P, Misteli T (2006) Lamin A-dependent nuclear defects in human aging. *Science* 312:1059–1063
- Shumaker DK, Dechat T, Kohlmaier A, Adam SA, Bozovsky MR, Erdos MR, Eriksson M, Goldman AE, Khuon S, Collins FS, Jenuwein T, Goldman RD (2006) Mutant nuclear lamin A leads to progressive alterations of epigenetic control in premature aging. *Proc Natl Acad Sci USA* 103:8703–8708
- Singh PB, Georgatos SD (2002) HP1: facts, open questions, and speculation. *J Struct Biol* 140:10–16
- Smallwood A, Estève PO, Pradhan S, Carey M (2007) Functional cooperation between HP1 and DNMT1 mediates gene silencing. *Genes Dev* 21:1169–1178
- Soille P (2004) Morphological image analysis, principles and applications, 2nd edn. Springer, Heidelberg
- Strašák L, Bártová E, Hamičarová A, Galiová G, Krejčí J, Kozubek S (2009) H3K9 acetylation and radial chromatin positioning. *J Cell Physiol* 220:91–101
- Taddei A, Maison C, Roche D, Almouzni G (2001) Reversible disruption of pericentric heterochromatin and centromere function by inhibiting deacetylases. *Nature Cell Biol* 3:114–120
- Ye Q, Worman HJ (1996) Interaction between an integral protein of the nuclear envelope inner membrane and human chromodomain proteins homologous to *Drosophila* HP1. *J Biol Chem* 271:14653–14656
- Yuan X, Feng W, Imhof A, Grummt I, Zhou Y (2007) Activation of RNA polymerase I transcription by cockayne syndrome group B protein and histone methyltransferase G9a. *Mol Cell* 27:585–595